ISSN: 2476-6909; Modares. Mech. Eng. *2026;26(09):697-706.*

Modares Mechanical Engineering

DOI: 10.48311/mme.2025.117363.82879
journal homepage: mme.modares.ac.ir

A Performance-Based Hybrid PSO-GA Framework for Optimal Process Noise Covariance Tuning in INS/GNSS Integration

Mohammad Hassan Najjarnasab, Hassan Salarieh*

Mechanical Engineering Department, Sharif University of Technology, Tehran, Iran.

ARTICLE INFO

Article Type
Original Research

Article History
Received: October 30, 2025
Revised: December 18, 2025
Accepted: December 18, 2025
ePublished: June 20, 2026

ABSTRACT

Accurate state estimation in INS/GNSS integrated navigation is critical, and its most common implementation, the Extended Kalman Filter (EKF), is highly dependent on the tuning of its process noise covariance matrix (Q). Conventional tuning methods, such as those based on stationary Allan-variance (AV) analysis, often fail to capture sensor behavior under real-world dynamic conditions, leading to filter inconsistency, sub-optimal accuracy, and poor dynamic response, such as overshoot upon GNSS re-acquisition. This paper proposes a novel, data-driven offline framework to optimize Q. Our approach parameterizes the continuous-time covariance (Q_c) using four physically meaningful scalars and tunes them using a hybrid Particle Swarm Optimization and Genetic Algorithm (PSO-GA). The optimization minimizes a performance-based objective function: the mean trajectory-wide Root Mean Square Error (RMSE) evaluated over a comprehensive set of sliding, pure-INS windows. Experimental validation on a real-world dataset demonstrates that the proposed tuning framework significantly outperforms conventional Allan-variance based tuning. Specifically, it reduces the mean terminal position and attitude errors by 52% and 84%, respectively, while simultaneously tightening the estimated error bounds by 59% and 82%, indicating superior filter consistency and robustness. Critically, in a simulated GNSS outage-and-recovery scenario, the proposed filter exhibited rapid, stable convergence without any overshoot, a significant improvement over the AV-tuned filter which suffered from severe overshoots. By directly linking the Q matrix parameters to observed navigation performance, this work provides a practical and robust methodology for EKF tuning.

Keywords: INS/GNSS integration, Extended Kalman Filter (EKF), Process noise covariance tuning, Hybrid PSO-GA, low-cost IMU.

How to cite this article
Najjarnasab M.H, Salarieh H, A Performance-Based Hybrid PSO-GA Framework for Optimal Process Noise Covariance Tuning in INS/GNSS Integration. Modares Mechanical Engineering; *2026;26(09):697-706.*

*Corresponding author's email: salarieh@sharif.edu
*Corresponding ORCID ID: 0000-0002-0604-5731

شاپا: ۷۹۰۹-۲۴۷۶؛ مهندسی مکانیک مدرس. ۷۰۶-۷۹۷ :(۰۹)۲۶؛۱۴۰۵

مهندسی مکانیک مدرس

DOI: 10.48311/mme.2025.117363.82879

صفحه اصلی مجله: mme.modares.ac.ir

ساختار هیبریدی PSO–GA مبتنی بر عملکرد برای تنظیم بهینه کوواریانس نویز فرآیند در تلفیق INS/GNSS

محمد حسن نجارنصب، حسن سالاریه*

دانشکده مهندسی مکانیک، دانشگاه صنعتی شریف، تهران، ایران

اطلاعات مقاله

نوع مقاله
مقاله پژوهشی

تاریخچه مقاله
دریافت: ۱۴۰۴/۰۸/۰۸
بازنگری: ۱۴۰۴/۰۹/۲۷
پذیرش: ۱۴۰۴/۰۹/۲۷
ارائه آنلاین: ۱۴۰۵/۰۳/۳۰

چکیده

تخمین دقیق حالت در ناوبری تلفیقی INS/GNSS از اهمیت بنیادین برخوردار است و متداول‌ترین ساختار آن، یعنی فیلتر کالمن توسعه‌یافته (EKF)، وابستگی زیادی به تنظیم ماتریس کوواریانس نویز فرایند (Q) دارد. روش‌های متعارف تنظیم، به‌ویژه مبتنی بر تحلیل واریانس آلن (AV) در شرایط ایستا، اغلب قادر به بازنمایی رفتار حسگر در شرایط دینامیکی واقعی نیستند و این امر به ناسازگاری فیلتر، دقت زیر بهینه و پاسخ دینامیکی نامطلوب، از جمله فراجهش هنگام بازیابی GNSS، منجر می‌شود. در این مقاله، چارچوبی داده‌محور و برون‌خط برای بهینه‌سازی Q ارائه شده است. در این رویکرد، کوواریانس زمان‌پیوسته (Qc) با چهار پارامتر اسکالر پارامتردهی شده و با الگوریتم ترکیبی بهینه‌سازی ازدحام ذرات و الگوریتم ژنتیک (PSO-GA) تنظیم می‌شود. بهینه‌سازی با کمینه‌سازی تابع هدفی مبتنی بر عملکرد انجام می‌شود که برابر با میانگین خطای ریشه میانگین مربعات (RMSE) در کل مسیر و محاسبه‌شده بر پنجره‌های لغزان INS خالص است. اعتبارسنجی تجربی نشان می‌دهد چارچوب پیشنهادی نسبت به تنظیم AV عملکرد بهتری دارد؛ به‌گونه‌ای که میانگین خطای نهایی موقعیت و وضعیت به‌ترتیب ۵۲٪ و ۸۴٪ کاهش یافته و همزمان کران‌های خطای برآوردی ۵۹٪ و ۸۲٪ فشرده‌تر شده‌اند که بیانگر سازگاری و پایداری برتر فیلتر است. همچنین در سناریوی شبیه‌سازی‌شده قطع و بازیابی GNSS، فیلتر پیشنهادی همگرایی سریع و پایدار بدون فراجهش نشان داد، در حالی‌که فیلتر تنظیم‌شده با AV دچار فراجهش بود. این پژوهش با ایجاد ارتباط مستقیم میان پارامترهای Q و عملکرد ناوبری مشاهده‌شده، روشی عملی و مقاوم برای تنظیم EKF ارائه می‌کند.

کلیدواژه‌ها: ناوبری تلفیقی INS/GNSS، فیلتر کالمن توسعه‌یافته (EKF)، تنظیم کوواریانس نویز فرآیند، بهینه‌سازی هیبرید PSO-GA، واحد اندازه‌گیری اینرسی کم‌هزینه

نحوه ارجاع به این مقاله

نجارنصب محمد حسن، سالاریه حسن، ساختار هیبریدی PSO–GA مبتنی بر عملکرد برای تنظیم بهینه کوواریانس نویز فرآیند در تلفیق INS/GNSS، مهندسی مکانیک مدرس. ۷۰۶-۷۹۷ :(۰۹)۲۶؛۱۴۰۵

*پست الکترونیکی نویسنده عهده‌دار مکاتبات: salarieh@sharif.edu

*شناسه ارکید نویسنده عهده‌دار مکاتبات: 0000-0002-0604-5731

1- Introduction

Tri-axial accelerometers and gyroscopes, integrated as an Inertial Measurement Unit (IMU), provide self-contained, high-rate measurements of specific force and angular rate and constitute the core sensing modality of strapdown inertial navigation across platforms. Yet their measurements carry stochastic errors (time-varying biases, random walks, colored noise) that are integrated during dead-reckoning, causing position, velocity, and attitude to drift with time. To arrest this growth, IMU data are routinely fused with absolute observations from GNSS in an Extended Kalman Filter (EKF), leveraging complementary strengths: short-term, high-bandwidth stabilization from the Inertial Navigation System (INS) and long-term, bounded accuracy from GNSS.

The effectiveness and even stability of this fusion hinges on how the filter models uncertainty. In practice, the process-noise covariance Q must be carefully tuned so that the INS prediction reflects realistic sensor noise and bias driving terms. Tuning Q is difficult for three reasons. First, IMU datasheet parameters are obtained under laboratory conditions and often deviate from in-field behavior. Second, once deployed, the apparent noise characteristics vary with operating conditions; vehicle vibration, temperature, and environmental factors such as road quality can alter the sensor's observed noise statistics. Third, manual trial-and-error offers no guarantee of appropriate Q tuning.; a mis-tuned Q yields inconsistency, slow convergence, or outright divergence.

This review surveys recent work along four complementary strands: (i) model-based, offline tuning for EKF-based INS/GNSS integration; (ii) adaptive/online estimation of process and measurement covariances; (iii) data-driven and metaheuristic strategies for tuning; and (iv) alternatives to EKF, notably factor-graph formulations. Within this structure, we position our contribution—a trajectory-level RMSE–driven tuning of Q using a hybrid PSO-GA search—as a bridge between static noise characterization and performance-linked tuning, complementing model-grounded approaches while addressing practical gaps in consistency and convergence under real operating conditions.

Model-based EKF tuning for INS/GNSS has shifted from ad-hoc hand setting toward data-linked procedures. For instance, structured frameworks have been proposed for tuning EKF parameters in both direct and indirect INS/GNSS integration, emphasizing the centrality of matching Q/R to sensor statistics and operating conditions [1]. Complementary work incorporates pseudo-measurement design or scenario-informed rules to stabilize tuning when GNSS is degraded; e.g., a multi-step pseudo-measurement adaptive KF improves robustness to environmental variability [2]. These studies collectively argue that principled tuning of Q materially affects consistency, convergence, and accuracy in integrated navigation.

A second strand adapts covariances online. Innovation-driven covariance matching and related adaptive methods continue to be extended to tightly coupled INS/GNSS and tracking sub-systems, showing tangible gains over fixed covariances in dynamic or weak-signal regimes [3,4]. Beyond conventional EKF structure, adaptive EnKF formulations and invariant EKFs with EM-style noise estimation have been explored to improve stability under nonlinearities and model mismatch [5,6]. Together, these works motivate tuning Q to data—either continuously online or via repeatable, data-driven offline procedures—rather than relying on static, a priori settings.

Noise characterization remains the bedrock for credible Q models. Recent Allan-variance (AV) analyses compare multiple MEMS grades and highlight how real-world noise departs from laboratory datasheets, underscoring the gap between nominal specs and field behavior [7]. Some studies revisit stochastic IMU modeling and reiterate that tuning should be anchored to statistics that reproduce the observed Allan signatures and operational conditions, not just static bench tests [8]. Our approach leverages this insight by parameterizing Q with a small set of physically meaningful scalars (accelerometer/gyro white noise and bias-drive terms) and judging each candidate by trajectory-wide RMSE under realistic motion.

A third line uses data-driven search and metaheuristics to tune Q (and sometimes R). Although many applications lie outside navigation, recent results consistently show that evolutionary search can reconcile accuracy and consistency without brittle heuristics: PSO/gradient hybrids for EKF noise estimation on vehicle data [9]; multi-objective GA tuning of EKF covariances for consistent state estimation [10]; PSO-assisted adaptive EKF and other metaheuristic variants for real-time parameter adjustment [11–13]. This evidence supports our choice of a hybrid PSO-GA: PSO concentrates the search rapidly [14]; GA injects diversity to avoid local minima [15]—an effective combination for a four-parameter, nonconvex Q-tuning landscape scored by RMSE and consistency metrics.

Finally, several works compare EKF-based INS/GNSS with factor-graph optimization (FGO). A widely cited study shows that FGO can outperform EKF in challenging settings by exploiting historical correlations and iterative re-linearization [16], with subsequent comparisons and extensions reporting accuracy/robustness gains in automotive and maritime contexts [17–19]. Efficient FGO variants continue to mature the tooling, though they often carry higher computational and implementation overhead than EKF [20,21]. In practice, EKF remains attractive for embedded real-time fusion—provided Q is well tuned—a perspective echoed in recent best-practice guidance for navigation filters [22]. Our contribution targets this practical gap: we keep the real-time EKF architecture but tune Q from data via an RMSE-based objective measured on sliding pure-INS windows initialized from an INS–GNSS reference, thereby linking the process-noise model directly to observed navigation performance and filter self-consistency.

Unlike prior metaheuristic tuning approaches that typically minimize innovation-based metrics or global estimation error (often masked by frequent measurement updates), our contribution introduces a pure-INS sliding-window objective function. This formulation explicitly evaluates the accuracy of the instantaneous state estimation, particularly the sensor biases, at every time step. Since inertial sensor biases are relatively stable over short intervals due to thermal inertia, any significant drift within a window is directly attributable to errors in the initial bias estimate. Therefore, minimizing the trajectory-wide windowed RMSE explicitly targets prediction drift and forces the filter to maintain precise state estimates continuously, ensuring reliable performance during GNSS outages rather than merely fitting the measurement updates.

2- System Model and Problem Statement

This section formalizes the navigation model and the estimation problem used in the rest of the paper. We first fix notation and coordinate frames, then summarize the strapdown INS mechanization for position, velocity, attitude, and sensor-bias dynamics. Next, we introduce the measurement models for GNSS and a lateral body-velocity constraint used as aiding. A centralized, error-state Kalman filter is then stated in continuous and discrete time. Finally, we define a compact, four-parameter block-diagonal parameterization of the continuous-time process-noise covariance $\mathbf{Q}_c$, along with its mapping to the discrete-time $\mathbf{Q}_d$; these parameters constitute the decision variables later optimized by the hybrid PSO-Genetic scheme.

2-1- Frames and Notation

We adopt four reference frames: inertial frame (i-frame), Earth-centered-Earth-fixed frame (e-frame), navigation frame (n-frame) — the local North–East–Down (NED) coordinate frame— and body (b-frame). A superscript denotes the frame in which a vector is resolved (e.g., $\mathbf{v}^n$ is velocity in n-frame). The direction-cosine matrix from body to navigation frame is $\mathbf{C}_b^n$, parameterized by the unit quaternion

q_b^n. Angular rates use the compact form ω_{xy}^z (rate of x with respect to y), resolved in the z-frame indicated by the superscript. These conventions are used consistently in what follows.

2-2- INS Mechanization

The strapdown INS mechanization propagates position, velocity, and attitude from IMU measurements. The INS state vector x is defined as:

$$x = [r^n, v^n, q_b^n]^T \tag{1}$$

where $\mathbf{r}^n = [\varphi \quad \lambda \quad h]^T$ denotes the geodetic position (latitude, longitude, altitude), $v^n = [v_N \quad v_E \quad v_D]^T$ is the velocity in NED frame, and $\mathbf{q}_b^n$ is the unit quaternion representing the body to navigation rotation. The nonlinear strapdown mechanization then reads:

$$\begin{bmatrix} \dot{r}^n \\ \dot{v}^n \\ \dot{q}_b^n \end{bmatrix} = \begin{bmatrix} D^{-1}v^n \\ C_b^n(f^b - b_a) - (2\omega_{ie}^n + \omega_{en}^n) \times v^n + g^n \\ \frac{1}{2} q_b^n \otimes \begin{bmatrix} 0 \\ \omega_{ib}^b - b_g - \omega_{in}^b \end{bmatrix} \end{bmatrix} \tag{2}$$

where C_b^n is the direction–cosine matrix obtained from the unit quaternion q_b^n, f^b and ω_{ib}^b are the IMU specific force and body angular rate, D maps the velocity in NED, v^n, to the geodetic rates, g^n is gravity in the n-frame, and b_a and b_g are the accelerometer and gyro biases, respectively. The inverse map D^{-1} converts geodetic rates back to velocity and, for a local ellipsoidal Earth model, is as follows:

$$D^{-1} = \begin{bmatrix} \frac{1}{M+h} & 0 & 0 \\ 0 & \frac{1}{(N+h)cos\varphi} & 0 \\ 0 & 0 & -1 \end{bmatrix} \tag{3}$$

Here M denotes the meridian radius of curvature and N denotes the prime-vertical radius of curvature of the reference ellipsoid. For further details, see [23,24].

2-2- Extended Kalman Filter Formulation

We employ an Extended Kalman filter (EKF) as the estimator that fuses strapdown INS propagation with absolute measurements from GNSS. The filter is formulated in the error state, which collects navigation errors and inertial-sensor bias errors as:

$$\delta x = \left[\delta r^n, \delta v^n, \delta\theta, \delta b_g, \delta b_a\right]^T \tag{4}$$

where δr^n and δv^n are the position and velocity errors in the n-frame, $\delta\theta$ is the small attitude error, representing the roll ($\delta\phi$), pitch ($\delta\theta$) and yaw ($\delta\psi$) errors, and δb_a, δb_g are the accelerometer and gyroscope bias errors. The attitude of the nominal solution is kept in the unit quaternion q_b^n, while $\delta\theta$ represents a small-angle correction to that quaternion. The continuous-time linearized error dynamics in general form are written as:

$$\delta\dot{x} = F\delta x + Gw, \qquad w \sim \mathcal{N}(0, Q_c) \tag{5}$$

where $F(t)$ is the error-dynamics matrix obtained by linearizing the INS mechanization, $G(t)$ is the noise input matrix, and $w(t)$ collects the white driving processes associated with inertial sensor noise and bias drift. The driving processes are zero-mean and mutually independent, with continuous-time covariance Q_c. Over the sampling interval Δt, the model is discretized to obtain the state-transition matrix $\Phi_k \approx I + F\Delta t$ and the discrete process covariance Q_d consistent with Q_c and Δt. For real-time deployment of the Kalman filter, the continuous-time model is discretized over a constant sampling interval Δt; the resulting discrete-time state, measurement equations and the discrete-time process covariance from continues-time process covariance obtained from below relations. This formulation assumes the resulting discrete process noise w_k and the measurement noise v_k are mutually uncorrelated.

$$\delta x_{k+1} = \Phi_k \delta x_k + G_k w_k, \qquad w_k \sim \mathcal{N}(0, Q_d) \tag{6}$$

$$\delta z_k = H_k \delta x_k + v_k, \qquad v_k \sim \mathcal{N}(0, R_k) \tag{7}$$

$$Q_d \approx G Q_c G \Delta t \tag{8}$$

In the Kalman filtering process [25], at each filter step, time propagation advances the error state and its covariance from time $k-1$ to k using the linear transition computed from the current nominal state and the sampling interval. This yields the prior (predicted) error estimate and covariance that represent the uncertainty accumulated during propagation:

$$\delta x_{k|k-1} = \delta\hat{x}_k^- = \Phi_k \delta x_{k-1|k-1} \tag{9}$$

$$P_{k|k-1} = P_k^- = F_k P_{k-1|k-1} F_k^T + G_k Q_k G_k^T \tag{10}$$

When a GNSS measurement is available, it is incorporated through a linear measurement model of the following form.

$$z_k^{GNSS} = H_k \delta x + v_k^{GNSS} \tag{11}$$

where H_k selects the observed components (typically position in the n-frame), and v_k^{GNSS} is zero-mean with covariance R_k^{GNSS}. The innovation r_k, compares the actual measurement against its prediction under the prior error estimate, computed from Eq. (12) and the innovation covariance is calculated from Eq. (13). The Kalman gain maps the innovation into a correction on the error states as formulated in Eq. (14). Finally, the error states and covariance matrix are updated through Eq. (15-16).

$$r_k = z_k - H_k \delta\hat{x}_k^- \tag{12}$$

$$S_k = H_k P_k^- H_k^T + R_k^{GNSS} \tag{13}$$

$$K_k = P_k^- H_k^T S_k^{-1} \tag{14}$$

$$\delta x_{k|k} = \delta\hat{x}_k^+ = \delta x_{k|k-1} + K_k\left(z_k - H_k \delta x_{k|k-1}\right) \tag{15}$$

$$P_{k|k} = P_k^+ = (I - K_k H_k) P_k^- (I - K_k H_k)^T + K_k R_k K_k^T \tag{16}$$

In Eq. (9–16), $\hat{x} \in \mathbb{R}^n$ denotes the state estimate and P is the estimated error covariance matrix. The superscripts "–" and "+" indicate a priori (predicted) and a posteriori (corrected) quantities, respectively. The covariance update in Eq. (16) employs the Joseph stabilized form, which helps ensure that P_k^+ remains positive definite.

2-3- Problem statement for Q tuning

This subsection formulates the identification of the process-noise covariance used by the INS/GNSS filter. The measurement covariance R_k^{GNSS} is read from the receiver; the goal is to determine a discrete-time process covariance Q_d that captures inertial sensor noise and bias driving terms while yielding consistent fusion performance.

We adopt a structure in which each 3×3 block is an identity scaled by a nonnegative scalar. This reflects the statistical independence of noise processes across the orthogonal axes of the tri-axial accelerometer and gyroscope sensors [26,27]. The decision vector is defined in Eq. (17), where the entries are constant (time-invariant) parameters for accelerometer noise, gyro noise, accelerometer-bias driving, and gyro-bias driving, respectively:

$$s = [s_a \quad s_g \quad s_{bg} \quad s_{ba}]^T \tag{17}$$

$$Q_c = \mathrm{diag}\left(s_a I_3, s_g I_3, s_{bg} I_3, s_{ba} I_3\right) \tag{18}$$

Although the framework permits optimizing a full matrix to account for potential cross-correlations, a diagonal structure is adopted here assuming independent noise across orthogonal axes.

2-4- Monte Carlo Evaluation Protocol

The randomized evaluation used to score each candidate process covariance proceeds as follows. For a given Q_d from Eq. (8,18) we (i) build a reference trajectory by running the INS–GNSS EKF with Q_d, (ii) perform multiple pure-INS over sliding windows initialized from that reference, and (iii) aggregate window errors across trials. Throughout, we use sampling frequency $f_s = 100$ Hz, window length $t_{win} = 300$ s and sliding time size $h_{hop} = 1$ s. With these definitions, the schedule uses strongly overlapping windows. The window selection and sliding-window are illustrated in Fig. 1.

Let $\mathcal{T} = \{1, \dots, N_T\}$ index Monte Carlo trials and $\mathcal{W}$ the set of sliding windows. Convert timing to number of samples via below relation.

$$n_{win} = \lfloor t_{win} f_s \rfloor, \quad n_{hop} = \lfloor h_{hop} f_s \rfloor \tag{19}$$

If k_w is the starting sample of window w, then its index set is $\mathcal{K}_w = \{k_w,\ k_w + 1,\ \dots\ ,\ k_w + n_{win} - 1\}$ with $k_{w+1} = k_w + n_{hop}$. At the start of each window, the pure-INS state is initialized from the INS–GNSS reference at k_w; the winAllan variancedow is then propagated using only IMU data with Eq. (2).

$$\begin{bmatrix} r^n_{k_w} \\ v^n_{k_w} \\ \theta_{k_w} \\ b_{g,k_w} \\ b_{a,k_w} \end{bmatrix}_{INS} := \begin{bmatrix} r^n_{k_w} \\ v^n_{k_w} \\ \theta_{k_w} \\ b_{g,k_w} \\ b_{a,k_w} \end{bmatrix}_{reference} \tag{20}$$

In Eq. (20), the pure-INS window inherits the instantaneous bias estimates $(\hat{b}_g, \hat{b}_a)$ from the reference trajectory at time k_w. During the short window duration ($t_{win} = 300$ s), these biases are held constant. This assumption is justified by the thermal inertia of the sensors, which prevents rapid bias shifts over short intervals.

We adopt Root Mean Square Error (RMSE) as the scoring metric because minimizing this error indicates that, in the reference trajectory computed with the candidate $\mathbf{Q}_c$, the INS/GNSS fusion is consistent and the filter converges rapidly. Each window inherits its initial condition from the reference; therefore, lower RMSE implies that the reference states (position, velocity, attitude and biases) have been well estimated under that $\mathbf{Q}_c$. Position RMSE for trial t and window w is computes as follows:

$$RMSE_w^{(t)} = \sqrt{\frac{1}{|\mathcal{K}_w|} \sum_{k \in \mathcal{K}_w} \left\| r_k^{n,\mathrm{INS}} - r_k^{n,\mathrm{referene}} \right\|_2^2} \tag{21}$$

The scalar objective function used for tuning Q_d is the mean RMSE over all windows and trials:

$$J(s) = \frac{1}{|\mathcal{T}||\mathcal{W}|} \sum_{t \in \mathcal{T}} \sum_{w \in \mathcal{W}} RMSE_w^{(t)} \tag{22}$$

where $|\cdot|$ denotes the cardinality, or the total number of elements. We chose RMSE because it is trajectory-wide and largely maneuver-agnostic. A single final terminal-error metric can fluctuate with path geometry, trial duration, and random noise realizations, making it an unstable indicator. By aggregating pointwise discrepancies over the entire trajectory (and across sliding windows), RMSE provides a more statistically robust measure of navigation accuracy for the pure-INS solution initialized from the INS–GNSS reference.

It is worth noting that while the objective function $J(s)$ is explicitly defined based on position RMSE, it implicitly constrains the velocity and attitude errors as well. Due to the integrative nature of INS mechanization, any persistent error in velocity, attitude, or sensor biases inevitably propagates into a growing position drift over the window duration. Therefore, minimizing the position RMSE effectively enforces the accuracy of all coupled upstream states without requiring a multi-objective formulation with arbitrary weighting factors.

We also assess filter consistency using its internally estimated uncertainty. At each time step, we take the one-sigma envelope from the diagonal of the predict-stage error covariance P (i.e., propagate P with pure-INS according to Eq. (10)). This self-reported envelope indicates how well the filter represents its own estimation error. The tuned continuous-time process covariance Q_c directly governs the growth of the prior covariance and therefore this metric. If the filter's predicted uncertainty is commensurate with the actual error (ideally slightly conservative, with only rare exceedances), that agreement serves as an additional, practical criterion indicating that Q_c is well tuned; A marked discrepancy between the estimated uncertainty and the actual error indicates a mis-tuned Q_c, resulting in either over-estimation (Q_c is too large) or under-estimation (Q_c is too small).

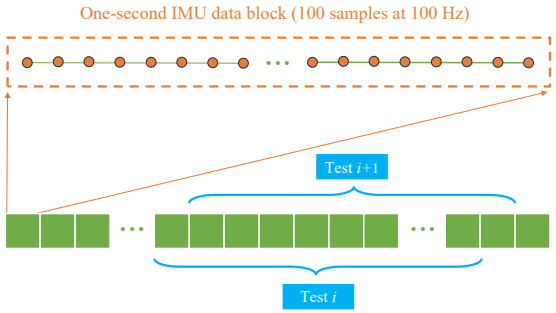

Fig. 1 Sliding-window selection and indexing for the Monte Carlo evaluation

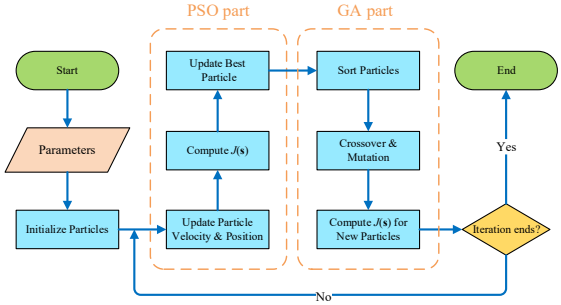

Fig. 2 Hybrid PSO-GA optimization workflow. The process initiates with 200 particles within the defined bounds. In each iteration, particles update positions via PSO dynamics to minimize the trajectory-wide RMSE objective function, $J(s)$. To prevent stagnation in local minima, a Genetic Algorithm operator is applied to the worst-performing subset of particles, utilizing crossover and mutation. This hybrid cycle repeats for 70 iterations to ensure convergence to the optimal Q_c parameters.

Table 1 hyperparameters of PSO-GA optimizer

Group	Name	Value	Note
Search	Minimum Value	$[10^{-6}, 10^{-12}, 10^{-16}, 10^{-15}]$	Lower bounds for s
	Maximum Value	$[10^{-2}, 10^{-4}, 10^{-6}, 10^{-5}]$	Upper bounds for s
PSO	Max Iterations	70	Iterations
	Population Size	200	Number of particles
	ϕ_1, ϕ_2	2.05, 2.05	Pre-constriction gains
	χ	0.72984	Constriction Coeff.
	c_1, c_2	$\chi\phi_1, \chi\phi_2$	Cognitive/Social
	w, w_{damp}	χ, 0.99	Inertia, Damping Ratio
	α	0.02	Max Velocity
GA	p_c	0.2	Crossover rate
	β	0.2	Blend range
	p_m	0.2	Mutation rate

2-5- Hybrid PSO-GA Optimization

We use a hybrid PSO-GA search to tune the four process-noise scalars defined in Eq. (17), because PSO rapidly concentrates the swarm around good regions, while periodic GA operators (blend crossover + mutation with elitism) inject diversity and reduce premature convergence. We adopt this hybrid because the problem requires estimating four continuous variables; in this setting it is more resilient to local minima, as PSO's rapid convergence and GA's exploratory search work in tandem to more effectively optimize $J(s)$. For a candidate s, we build Q_d from Q_c, run the INS–GNSS EKF to form the reference, evaluate pure-INS windows, and return $J(s)$. PSO updates positions and velocities of each particle with constriction, clamping, and reflection at bounds; then GA replaces a small worst subset using blend crossover (BLX-β) and random one-gene mutation. The selected hyperparameters for this

hybrid optimizer are reported in Table 1. Also the workflow of the hybrid PSO-GA algorithm is shown in Fig. 2.

3- Test and Experimental

To assess the proposed algorithm, we use a low-cost, consumer-grade IMU. The sensor was rigidly mounted on the test vehicle and driven along the trajectory shown in Figure 3. Prior to the dynamic tests, the IMU underwent a standard laboratory calibration to compensate for deterministic errors, including scale factors, misalignment, and turn-on biases. Consequently, the filter states $\delta\mathbf{b}_g$ and $\delta\mathbf{b}_a$ estimate only the stochastic in-run bias instabilities. Its noise characteristics were quantified via stationary (laboratory) Allan variance analysis [28]; results are summarized in Table 2. Data were logged, and the navigation solution was computed, at 100 Hz. The test vehicle's trajectory is shown in Figure 3. Data from the low-cost IMU were recorded at 100 Hz over a 30-minute session, during which the route in Figure 3 was traversed multiple times. The trajectory was intentionally motion-rich—featuring left/right turns (yaw excitation), altitude changes, and speed variations—providing sufficient excitation for state observability and rapid convergence of inertial-sensor biases and navigation states in the Kalman filter.

3- Results

This section presents quantitative and qualitative results for the proposed Q tuning method. We first outline the evaluation protocol and baselines, then report trajectory-wide RMSE improvements (accuracy), filter-consistency diagnostics (predicted covariance versus realized error), and the convergence behavior of Q tuned with the hybrid PSO-GA optimization.

3-1- Optimization Convergence

The Q tuning optimization operates on real sensor data. First, the required dataset is collected and logged as in Fig. 3; these recordings then serve as input to the offline search. Using the objective function in Eq. (22), the hybrid PSO-GA minimizes the trajectory-wide error metric over the four-dimensional Q parameterization. To verify the robustness and repeatability of the proposed scheme, the optimization process was executed multiple times with different random seeds. The results exhibited negligible variance in the final converged parameters, confirming that the chosen population size and hybrid mechanism effectively prevent entrapment in local minima.

Figure 4 plots the per-iteration objective—mean, windowed RMSE $J(\mathbf{s})$ from Eq. (22)—for this sensor. In each run, RMSE decreases rapidly over the initial iterations and then exhibits diminishing improvements before settling to a stable plateau, indicating convergence of RMSE under the hybrid PSO-GA search. The best-so-far and population-mean curves show consistent descent without oscillatory behavior or premature stagnation, confirming that the optimizer reliably reduces RMSE and stabilizes within the allotted iteration budget for both datasets. The final optimized parameters obtained from this search are reported in Table 3.

3-2- Evaluation of the Tuned Q

We now analyze the Q obtained by the optimization to validate that it yields credible state estimates. A well-tuned Q should (i) minimize navigation error and (ii) produce an internally consistent uncertainty forecast. The first aspect is enforced inside the optimizer itself by minimizing the trajectory-wide RMSE objective in Eq. (22). Because each pure-INS window is initialized from the INS–GNSS reference built with the same candidate Q_c (see Eq. (20)), a lower RMSE indicates that the reference states—and hence the window initial conditions—are well estimated under that Q.

The second aspect concerns the filter's own error prediction. With the tuned Q, the EKF's prior covariance P should propagate to realistic one-sigma bounds for position, velocity, and attitude at the end of each 5-minute window. We summarize those "final estimated errors" from the diagonal of P by taking the Euclidean norm of the relevant one-sigma components:

$$\hat{\sigma}_{Pos} = \left\| \begin{bmatrix} \sqrt{P_{11}} \\ \sqrt{P_{22}} \\ \sqrt{P_{33}} \end{bmatrix} \right\|_2 , \hat{\sigma}_{Vel} = \left\| \begin{bmatrix} \sqrt{P_{44}} \\ \sqrt{P_{55}} \\ \sqrt{P_{66}} \end{bmatrix} \right\|_2 , \hat{\sigma}_{Att} = \left\| \begin{bmatrix} \sqrt{P_{77}} \\ \sqrt{P_{88}} \\ \sqrt{P_{99}} \end{bmatrix} \right\|_2 \quad (23)$$

Here P_{ij} is the diagonal element of EKF prior estimated error covariance matrix, P, at the terminal time of the window; the first three diagonal entries correspond to position, the next three to velocity, and the next three to attitude states.

Table 2 Allan variance analysis of IMU

IMU	Accelerometer			Gyroscope		
	Random Walk $(m/s/\sqrt{hr})$	Bias stability (mg)	Output noise (mg)	Random Walk $(Deg/\sqrt{hr})$	Bias stability (Deg/hr)	Output noise (Deg/s)
Low-Cost	0.029	0.08	1.31	0.26	5.5	0.137

Table 3 Optimized process-noise parameters ($\mathbf{s}$) for the low-cost IMU.

Parameter	$\mathbf{s_a}$	$\mathbf{s_g}$	$\mathbf{s_{bg}}$	$\mathbf{s_{ba}}$
Optimized Value	3.475×10^{-3}	2.061×10^{-8}	3.664×10^{-12}	$\mathbf{7.758 \times 10^{-8}}$

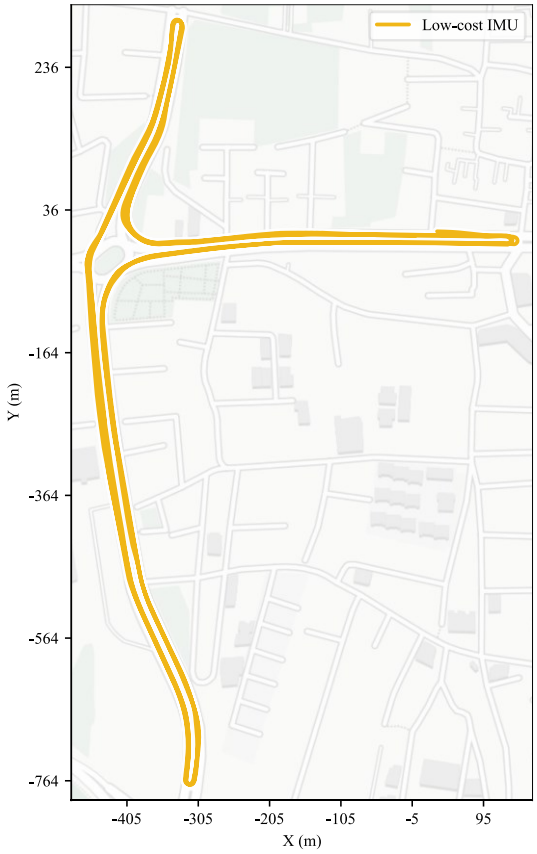

Fig. 3 Test vehicle trajectory used for evaluation. A low-cost IMU was rigidly mounted and logged at 100 Hz during a 30-minute session; the route was driven multiple times.

Additionally, we formed a conventional baseline by tuning Q from the stationary Allan-variance characterization reported in Table 2. Using those parameters, we constructed Q_d from Q_c and ran the identical Monte Carlo evaluation (same windows, hop, and scoring). Figures 5–6 visualize the distributions of final true errors for position, velocity, and attitude across all Monte Carlo windows alongside the filter's predicted one-sigma bounds $\hat{\sigma}_{\mathrm{Pos}}, \hat{\sigma}_{\mathrm{Vel}}, \hat{\sigma}_{\mathrm{Att}}$, enabling a direct comparison between realized performance and propagated uncertainty. With the PSO-GA tuned Q, the predicted bounds are slightly conservative and closely follow the empirical distributions, and indicating a good match between uncertainty error propagation and actual error; with the AV–tuned Q, the bounds are substantially larger than the realized errors (systematic over-estimation of uncertainty), indicating a mis-tuned covariance under in-motion conditions.

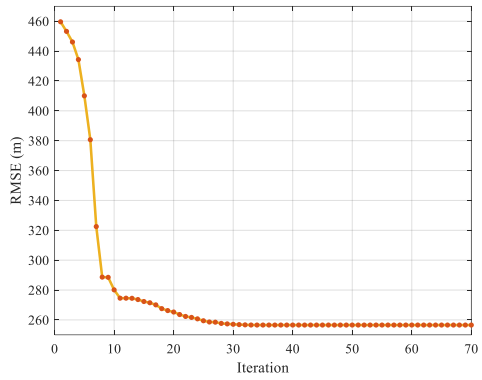

Fig. 4 Convergence of the hybrid PSO-GA tuning: per-iteration mean windowed RMSE $J(\mathbf{s})$ for the low-cost IMU.

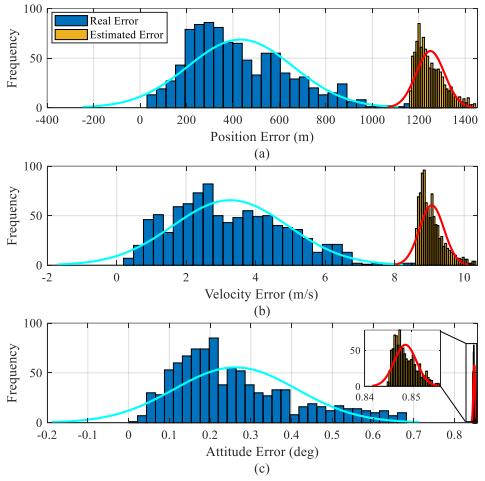

Fig. 5 Final error versus estimated final error the PSO-GA tuned Q: histograms over all sliding windows for (a) position, (b) velocity, and (c) attitude.

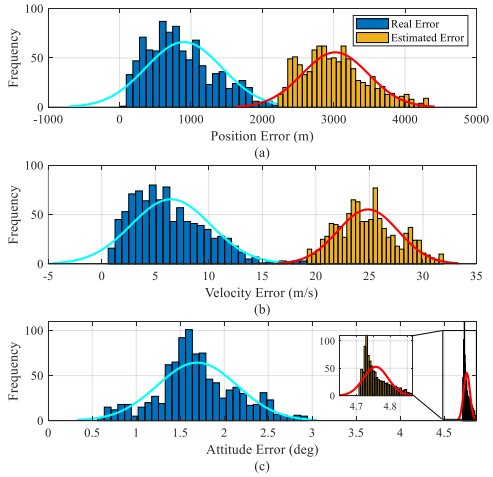

Fig. 6 Final error versus estimated final error under the AV tuned **Q**: histograms over all sliding windows for (a) position, (b) velocity, and (c) attitude.

Table 4 Terminal errors and estimated error for different tuning cases.

Metric	PSO-GA tuning		Allan-variance tuning	
	Mean	STD	Mean	STD
Position Error (m)	432.35	226.50	901.17	534.94
$\hat{\sigma}_{\text{Pos}}$ (m)	1249.94	61.10	3022.58	464.21
Velocity Error (m/s)	3.27	1.65	6.46	3.7
$\hat{\sigma}_{\text{Vel}}$ (m/s)	9.06	0.35	24.87	2.81
Attitude Error (deg)	0.26	0.15	1.69	0.45
$\hat{\sigma}_{\text{Att}}$ (deg)	0.84	0.002	4.75	0.036

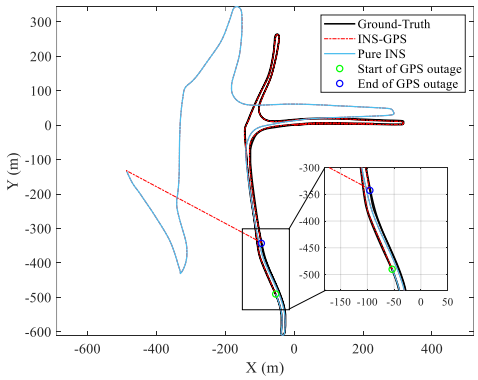

Fig. 7 2D trajectory scenario for evaluating the performance of tuning cases. This trajectory is obtained by PSO-GA tuned Q.

Table 4 summarizes, for each window endpoint, both the realized errors and the EKF's predicted one-sigma values under the proposed tuned Q and under the AV–derived baseline. This table reports lower final true errors for position, velocity, and attitude when using the proposed PSO-GA tuned Q than with the Allan-based baseline, implying more accurate estimation of the navigation states and biases by the EKF.

3-3- Filter Convergence Speed and Error Estimation

To evaluate generalization on data unseen during optimization, we selected a held-out interval from the low-cost IMU dataset and ran two configurations: (i) the proposed EKF with the PSO-GA tuned Q, and (ii) an EKF using Q obtained from Allan-variance analysis. Both configurations were given an identical initial convergence period period of 3 minutes with GNSS available to allow convergence from biased initial conditions. Immediately thereafter, GNSS was withheld for a 5-minute window to emulate a GNSS-denied segment. For visual context, the corresponding 2D trajectory for this scenario is shown in Fig. 7; this solution was generated using the PSO-GA tuned Q.

During the outage, the navigation solution devolves to pure INS; we therefore track the instantaneous errors in position, velocity, and attitude relative to the INS–GNSS reference, and the EKF's predicted one-sigma bounds propagated from the prior covariance P. This protocol allows a paired assessment of two properties: convergence speed before the outage (how quickly biases and states settle) and credibility during the outage (how well the predicted uncertainty matches the realized drift).

Figures 8–10 plot the component-wise navigation-state errors under the proposed PSO-GA tuned Q. GNSS is available during 0–3 min (initial convergence period), withheld from 3–8 min to emulate a GNSS-denied interval, and re-enabled for 8–9 min so that post-outage re-convergence is visible. For comparison, Fig. 11–13 show the corresponding state-error when the EKF uses the AV tuned Q. Both configurations use the same initial conditions and the same timing schedule to ensure a fair comparison.

Although a specific interval is visualized here for detailed analysis, this outage-and-recovery scenario was evaluated at multiple distinct segments along the trajectory, consistently yielding similar convergence behavior and overshoot suppression.

As seen in Fig. 8–10, the EKF achieves rapid convergence during the initial GNSS-aided phase. Throughout the 3–8 min GNSS outage, the realized errors remain within the predicted 1σ bounds, indicating credible uncertainty propagation under the PSO-GA tuned Q. When GNSS is restored at $t = 480$ s, all state errors (position, velocity, attitude) return to near zero without overshoot. Together, these observations indicate that the tuned Q provides both fast convergence and a reliable estimate of filter uncertainty, thereby supporting accurate and stable state estimation. In contrast, with the AV tuned Q, deficiencies are evident in Fig. 11–13. In Fig. 11, the altitude error exits the one-sigma band during the GNSS outage. In Fig. 12, all three velocity estimation error components ($\delta v_N, \delta v_E$ and δv_D) exhibit overshoot when GNSS is restored at $t = 480$ s; moreover, δv_D fails to settle during the initial convergence period, and its predicted uncertainty under-covers the realized error. Figure 13

likewise shows overshoot in the attitude estimation errors upon re-acquisition, consistent with mis-tuned process noise covariance.

4- Discussion

The results presented in this study highlight a significant discrepancy between standard laboratory-based tuning methods and the performance requirements of in-field, dynamic navigation. The AV derived Q, a conventional benchmark, was shown to be systematically over-conservative. This leads to a filter that reports far more uncertainty than it actually encounters and, more critically, exhibits poor dynamic response—specifically, significant overshoot upon GNSS re-acquisition—due to its over-reliance on GNSS measurements and distrust of its own IMU-driven propagation.

In contrast, the proposed PSO-GA tuning method, which optimizes Q directly against a trajectory-wide RMSE metric, yields a filter that is both accurate and consistent. The resulting Q produces error bounds that credibly bound the realized errors and facilitates rapid, stable convergence without the overshoots seen in the AV tuned filter. This demonstrates the superiority of a performance-linked tuning approach that captures the sensor's behavior under real operating conditions.

It is acknowledged that the proposed offline optimization, leveraging a hybrid PSO-GA search, carries a substantial computational burden. Specifically, the optimization process for the reported dataset required approximately 6 hours of wall-clock time utilizing parallel processing on an Intel Core i9-14900K processor (24 cores). While this duration is acceptable for a one-time offline characterization, it primarily reflects the overhead of the research-grade MATLAB (interpreted) environment. For routine industrial deployment, significant acceleration is achievable. Benchmarks on similar iterative estimation algorithms demonstrate that porting to C++ typically yields a 10-fold speedup [29], while leveraging GPU acceleration for parallel filter banks can improve throughput by several orders of magnitude [30]. Such enhancements would reduce the tuning time to minutes, rendering the framework highly efficient for industrial navigation.

However, this cost is justified in several practical scenarios where traditional methods fall short. This approach is invaluable for sensors lacking comprehensive datasheets or where AV test results are unavailable. Moreover, as our results imply, even when AV data is available, it may be inadequate. Real-world vehicle dynamics, encompassing significant vibrations and thermal fluctuations, deviate markedly from the static laboratory conditions of an AV test. In these cases, our method provides a data-driven path to a Q matrix that reflects the sensor's true operational noise characteristics.

This fine-tuning becomes particularly critical in advanced multi-sensor fusion architectures. When integrating INS with other sensors (e.g., odometers, magnetometers) or with pseudo-measurements (e.g., non-holonomic constraints), the corresponding measurement noise covariance (R) is often uncertain or difficult to model accurately. The Kalman filter's ability to optimally weigh these auxiliary measurements depends entirely on a correctly propagated state covariance P, which is directly governed by Q. If Q is mis-tuned (as with the AV baseline), the filter's state estimation will be suboptimal, failing to correctly fuse all available information. The proposed method, by grounding Q in observed navigation performance, provides the robust and reliable foundation necessary for these complex integration scenarios to achieve their full potential. Future work will extend this validation to standard commercial-grade sensors to confirm broader generalizability.

4- Conclusion

This paper addressed the critical challenge of process-noise covariance Q tuning for INS/GNSS integration, highlighting the pronounced limitations of conventional static methods, such as Allan variance, when applied to dynamic, real-world operating conditions. We proposed and validated a novel, data-driven offline optimization framework utilizing a hybrid PSO-GA optimization framework. This methodology optimizes the four key parameters of the continuous-time process noise covariance Q_c not against static sensor specifications, but by minimizing a performance-based objective function: the mean trajectory-wide RMSE evaluated over a comprehensive set of sliding, pure-INS windows. Experimental results using a low-cost IMU confirmed the efficacy of this approach. By forcing the filter to minimize drift over hundreds of short windows, the optimizer effectively tuned the system to maintain highly accurate instantaneous state estimates.

Consequently, numerical results indicate a substantial improvement in navigation performance. The optimized filter reduces terminal position and attitude errors by 52% and 84%, respectively, compared to standard AV-based tuning. Furthermore, the estimated error covariance bounds were reduced by 59% (position) and 82% (attitude), confirming that the proposed framework yields a more robust and consistent estimation. Furthermore, it successfully resolved the systematic over-conservatism inherent in the Allan-variance method; the proposed filter was shown to be highly consistent, with its predicted one-sigma uncertainty bounds credibly and tightly bounding the realized navigation errors. Most critically, the new tuning method yielded a filter with a robust and stable dynamic response. In a simulated GNSS outage-and-recovery scenario, the PSO-GA tuned filter exhibited rapid, stable convergence without any overshoot upon GNSS re-acquisition, in sharp contrast to the AV tuned filter which suffered from significant overshoots in velocity and attitude. By directly linking the Q matrix parameters to observed navigation performance, this work provides a practical and robust methodology for tuning the EKF, yielding a filter that is not only more accurate but also demonstrably more consistent and stable for real-world navigation tasks.

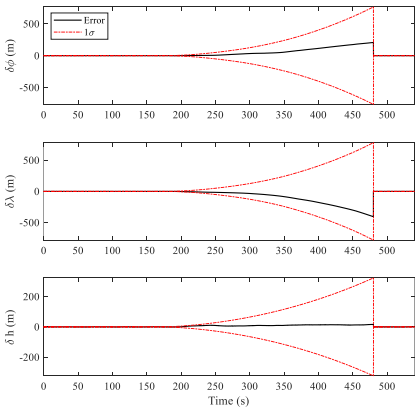

Fig. 8 Position-state errors (δφ, δλ, δh) with PSO-GA tuned Q.

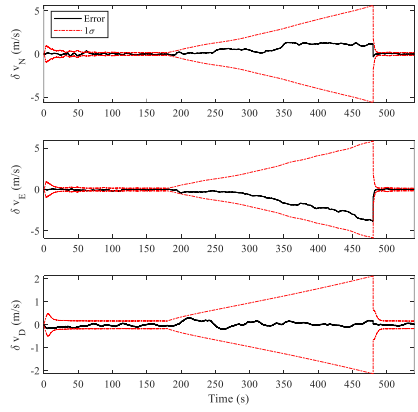

Fig. 9 Velocity-state errors ($\delta v_N, \delta v_E, \delta v_D$) with PSO-GA tuned Q.

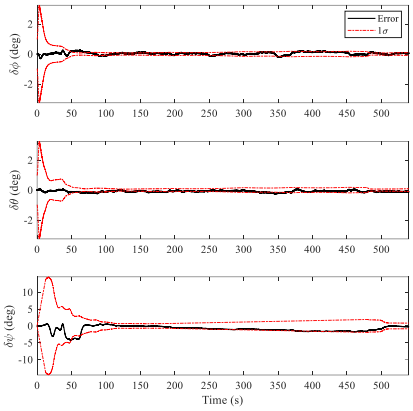

Fig. 10 Attitude-state errors ($\delta\phi, \delta\theta, \delta\psi$) with PSO-GA tuned Q.

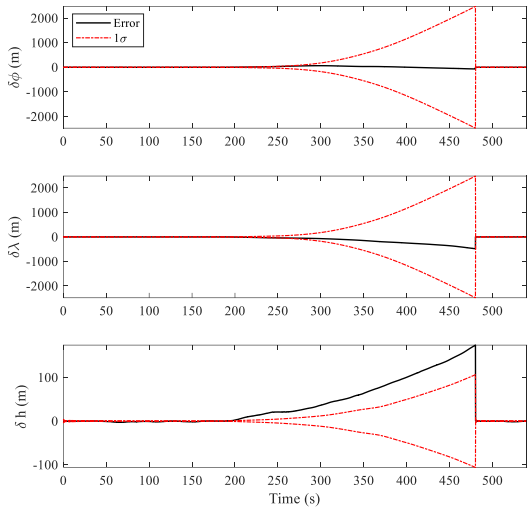

Fig. 11 Position-state errors (δφ, δλ, δh) with AV tuned Q.

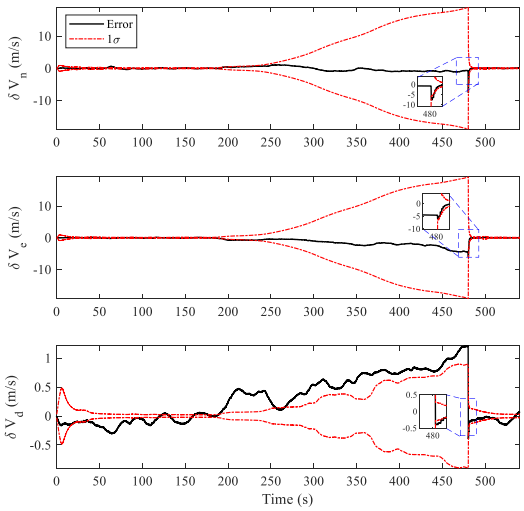

Fig. 12 Velocity-state errors ($\delta v_N, \delta v_E, \delta v_D$) with AV tuned Q.

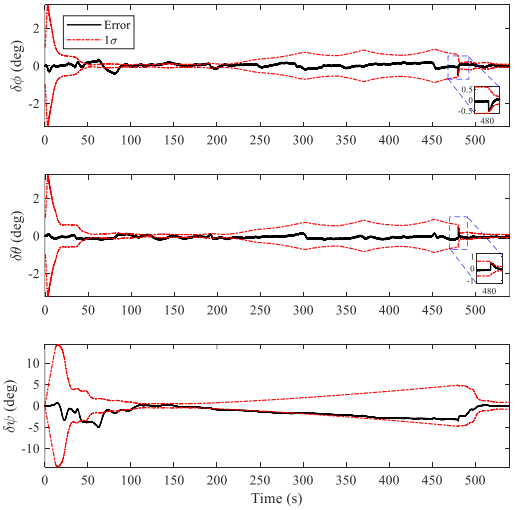

Fig. 13 Attitude-state errors ($\delta\phi, \delta\theta, \delta\psi$) with AV tuned Q.

Ethics Approval

The scientific content of this article is the result of the authors' research and has not been published in any Iranian or international journal.

Conflict of Interest

There are no other conflicts of interest to declare.

References

[1] A. J. A. Tavares Jr and N. M. F. Oliveira, "A Novel Approach for Kalman Filter Tuning for Direct and Indirect Inertial Navigation System/Global Navigation Satellite System Integration," *Sensors*, vol. 24, no. 22, p. 7331, 2024. doi: 10.3390/s24227331

[2] D. Wang and H. Zhang, "A multi-step pseudo-measurement adaptive Kalman filter based on filtering performance evaluation and its application in the ins/gnss navigation system," *Remote Sens (Basel)*, vol. 16, no. 5, p. 926, 2024. doi: 10.3390/rs16050926

[3] Y. Cheng, S. Zhang, X. Wang, H. Wang, and H. Yang, "Kalman Filter with Adaptive Covariance Estimation for Carrier tracking under weak signals and dynamic conditions," *Electronics (Basel)*, vol. 13, no. 7, p. 1288, 2024. doi: 10.3390/electronics13071288.

[4] Y. Yuan, F. Li, J. Chen, Y. Wang, and K. Liu, "An improved Kalman filter algorithm for tightly GNSS/INS integrated navigation system," *Math. Biosci. Eng*, vol. 21, pp. 963–983, 2024. doi:10.3934/mbe.2024040.

[5] Z. Liang *et al.*, "An Enhanced Adaptive Ensemble Kalman Filter for Autonomous Underwater Vehicle Integrated Navigation," *Drones*, vol. 8, no. 12, p. 711, 2024. doi: 10.3390/drones8120711.

[6] Y. Pandey, R. Bhattacharyya, and Y. N. Singh, "Adaptive Invariant Extended Kalman Filter with Noise Covariance Tuning for Attitude Estimation," *ArXiv*, 2024. doi: 10.48550/arXiv.2410.01958.

[7] V. Suvorkin, M. Garcia-Fernandez, G. González-Casado, M. Li, and A. Rovira-Garcia, "Assessment of noise of mems imu sensors of different grades for gnss/imu navigation," *Sensors*, vol. 24, no. 6, p. 1953, 2024. doi: 10.3390/s24061953.

[8] A. Shahrawy *et al.*, "Breaking Through GNSS Outage: Advanced Stochastic Model for MEMS IMU in Navigation,"

IEEE J Sel Top Appl Earth Obs Remote Sens, 2025. doi: 10.1109/JSTARS.2025.3581379.
[9] S. F. G. Ehlers, P. Sourkounis, Z. Ziaukas, J.-P. Kobler, and H.-G. Jacob, "Optimized Tuning of an EKF for State and Parameter Estimation in a Semitrailer," 2024. doi: 10.15488/17784.
[10] M. Theiler, D. Schneider, and C. Endisch, "Kalman filter tuning using multi-objective genetic algorithm for state and parameter estimation of lithium-ion cells," *Batteries*, vol. 8, no. 9, p. 104, 2022. doi: 10.3390/batteries8090104.
[11] X. Lu, M. Chen, and Y. Tian, "Accurate state-of-charge estimation of LiFePO4 battery: An adaptive extended kalman filter approach using particle swarm optimization," *Energy Reports*, vol. 14, pp. 1169–1178, 2025. doi: 10.1016/j.egyr.2025.07.023.
[12] N. Nernchad, K. Buakham, P. Janthirat, M. Janchuen, and U. Prasatsap, "A modified artificial hummingbird algorithm tuning optimal process noise covariance and measurement noise covariance for the Kalman filter in the noise reduction analysis of steering angle sensors in small electric vehicle," *Measurement*, p. 117984, 2025. doi: 10.1016/j.measurement.2025.117984.
[13] E. Mohajeri, S. H. Pourtakdoust, and F. Pazooki, "A neural-metaheuristic kalman filter for moving microburst wind shear identification," *J Franklin Inst*, vol. 362, no. 1, p. 107390, 2025. doi: 10.1016/j.jfranklin.2024.107390.
[14] M. R. Bonyadi and Z. Michalewicz, "Particle swarm optimization for single objective continuous space problems: a review," *Evol Comput*, vol. 25, no. 1, pp. 1–54, 2017. doi: 10.1162/EVCO_r_00180.
[15] S. Katoch, S. S. Chauhan, and V. Kumar, "A review on genetic algorithm: past, present, and future," *Multimed Tools Appl*, vol. 80, no. 5, pp. 8091–8126, 2021. doi: 10.1007/s11042-020-10139-6.
[16] W. Wen, T. Pfeifer, X. Bai, and L.-T. Hsu, "Factor graph optimization for GNSS/INS integration: A comparison with the extended Kalman filter," *NAVIGATION: Journal of the Institute of Navigation*, vol. 68, no. 2, pp. 315–331, 2021. doi: 10.1002/navi.421.
[17] S. Xin, X. Wang, J. Zhang, K. Zhou, and Y. Chen, "A comparative study of factor graph optimization-based and extended Kalman filter-based PPP-B2b/INS integrated navigation," *Remote Sens (Basel)*, vol. 15, no. 21, p. 5144, 2023. doi: 10.3390/rs15215144.
[18] B. Ning, F. Zhao, H. Luo, D. Luo, and W. Shao, "Robust GNSS/INS Tightly Coupled Positioning Using Factor Graph Optimization with P-Spline and Dynamic Prediction," *Remote Sens (Basel)*, vol. 17, no. 10, p. 1792, 2025. doi: 10.3390/rs17101792.
[19] Y. Hu, H. Li, and W. Liu, "Robust factor graph optimisation method for shipborne GNSS/INS integrated navigation system," *IET Radar, Sonar & Navigation*, vol. 18, no. 5, pp. 782–798, 2024. doi: 10.1049/rsn2.12521.
[20] Z. Yang, X. Ding, Y. Yang, and Q. Wang, "OiSAM-FGO: an efficient factor graph optimization algorithm for GNSS/INS integrated navigation system," *Satellite Navigation*, vol. 6, no. 1, p. 23, 2025. doi: 10.1186/s43020-025-00173-w.
[21] C. Taylor and J. Gross, "Factor graphs for navigation applications: A tutorial," *NAVIGATION: Journal of the Institute of Navigation*, vol. 71, no. 3, 2024. doi: 10.33012/navi.653.
[22] J. R. Carpenter and C. N. D'Souza, "Navigation filter best practices," 2025.
[23] P. Aggarwal, Z. Syed, and N. El-Sheimy, *MEMS-based integrated navigation*. Artech House, 2010.
[24] P. Groves, *Principles of GNSS, Inertial, and Multisensor Integrated Navigation Systems, Second Edition*. 2013.
[25] D. Simon, *Optimal state estimation: Kalman, H infinity, and nonlinear approaches*. John Wiley & Sons, 2006.
[26] D. Engelsman, Y. Stolero, and I. Klein, "Parametric and state estimation of stationary MEMS-IMUs: A tutorial," *arXiv:2307.08571*, 2023. doi: 10.1109/ACCESS.2024.3476145.
[27] A. Shahrawy *et al.*, "Breaking Through GNSS Outage: Advanced Stochastic Model for MEMS IMU in Navigation," *IEEE J Sel Top Appl Earth Obs Remote Sens*, 2025. doi: 10.1109/JSTARS.2025.3581379.
[28] N. El-Sheimy, H. Hou, and X. Niu, "Analysis and modeling of inertial sensors using Allan variance," *IEEE Trans Instrum Meas*, vol. 57, no. 1, pp. 140–149, 2008. doi: 10.1109/TIM.2007.908635.
[29] M. Ruiz *et al.*, "Acceleration of an algorithm based on the maximum likelihood bolometric tomography for the determination of uncertainties in the radiation emission on jet using heterogeneous platforms," *Applied Sciences*, vol. 12, no. 13, p. 6798, 2022. doi: 10.3390/app12136798.
[30] X. Ai, G. Mania, H. M. Gray, M. Kuhn, and N. Styles, "A GPU-based Kalman Filter for track fitting," *Comput Softw Big Sci*, vol. 5, no. 1, p. 20, 2021, doi: 10.1007/s41781-021-00065-z. doi: 10.1007/s41781-021-00065-z.